Structure of the connexin-43 gap junction channel reveals a closed sieve-like molecular gate

Chao Qi[1,2,#], Silvia Acosta-Gutierrez[3,#], Pia Lavriha[1,2], Alaa Othman[4], Diego Lopez-Pigozzi[5,6], Erva Bayraktar[6], Dina Schuster[1,2,4], Paola Picotti[4], Nicola Zamboni[4], Mario Bortolozzi[5,6], Francesco L. Gervasio[7,8,9*] and Volodymyr M. Korkhov[1,2*]

[1] Institute of Molecular Biology and Biophysics, ETH Zurich, Switzerland

[2] Laboratory of Biomolecular Research, Paul Scherrer Institute, Villigen, Switzerland

[3] Institute for the Physics of Living Systems, Institute of Structural and Molecular Biology, and Department of Chemistry. University College London, London, UK

[4] Institute of Molecular Systems Biology, ETH Zurich, Switzerland

[5] Department of Physics and Astronomy "G. Galilei", University of Padova, Padua, Italy

[6] Veneto Institute of Molecular Medicine (VIMM), Padua, Italy

[7] Department of Chemistry, University College London, WC1E 6BT London, UK

[8] School of Pharmaceutical Sciences, University of Geneva, CH-1211 Geneva, Switzerland

[9] ISPSO, University of Geneva, CH-1211 Geneva, Switzerland

[*] Corresponding authors: francesco.gervasio@unige.ch, volodymyr.korkhov@psi.ch

[#] These authors contributed equally

Abstract

Gap junction channels (GJCs) mediate intercellular communication by connecting two neighboring cells and enabling direct exchange of ions and small molecules. Cell coupling via connexin-43 (Cx43) GJCs is important in a wide range of cellular processes in health and disease [1-3], yet the structural basis of Cx43 function and regulation has not been determined until now. Here we describe the structure of a human Cx43 GJC solved by cryo-EM and single particle analysis at 2.26 Å resolution. The pore region of Cx43 GJC features several lipid-like densities per Cx43 monomer, located close to a putative lateral access site at the monomer boundary. We found a previously undescribed closed sieve-like gate on the cytosolic side of the pore, formed by the N-terminal domain and the transmembrane helix 2 of Cx43 and stabilized by a small molecule. Structures of the Cx43 GJC and hemichannels in nanodiscs confirm the sieve-like gate arrangement. The features of the Cx43 GJC and hemichannel cryo-EM maps and the channel properties revealed by molecular dynamics simulations suggest that the captured states of Cx43 are closed.

Introduction

Gap junction (GJ) mediated intercellular communication is one of the major pathways of information exchange between the cells. GJs are specialized regions of the plasma membrane at the cell-cell interface that link two adjacent cells and establish their metabolic and electrical coupling [4]. Connexins are the building blocks of the GJ channels (GJCs) which belong to a group of large-pore channels. This group includes a number of structurally related (innexins, pannexins, LRRC8) and unrelated proteins (CALHM) [5]. A total of 21 connexin genes have been identified in the human genome [6]. The 43 kDa connexin-43 (Cx43, gene name *GJA1*) was identified as a major constituent of rat heart GJs in 1987 [7], and it is arguably one of the most extensively studied connexins. Like all connexin homologues, Cx43 monomers assemble into hexameric hemichannels (HCs), also known as connexons. HCs that reach the plasma membrane of one cell interact with their counterparts on the neighboring cell, forming GJCs, typically organized into hexagonal arrays at the intercellular interface [8]. GJCs enable direct metabolic and electric coupling between the cells, facilitating the passage of ions, small molecules, metabolites, peptides and other cellular components below a size threshold of approximately 1.5 kDa [9]. GJCs formed by Cx43 are crucial for a wide range of physiological processes, from propagation of heart action potentials [3] to maintenance of neuro-glial syncytium [2] and skin wound healing [1]. The clinical importance of Cx43 is highlighted by mutations linked to several genetic disorders, such as oculodentodigital dysplasia (ODDD) [10-12], hypoplastic left heart syndrome 1 [13], Hallermann-Streiff syndrome [14], atrioventricular septal defect 3 [13], etc., and by recognition of the protein as a drug target for treatment of cancer, skin wounds, eye injury and inflammation and cardiac arrhythmias (reviewed by Laird and Lampe [9]).

Much of what we know today about the molecular biology, electrophysiological properties and regulation of connexin gap junctions has been derived from the studies on Cx43 (reviewed in [15]). Early attempts to characterize the structure of Cx43 using cryo-electron microscopy (cryo-EM) of 2D crystals produced low resolution reconstructions [16]. More recently, several homologous connexin GJCs and HCs have been structurally characterized at high resolution, using X-ray crystallography and cryo-EM. The structures of Cx26 [17] and Cx46/50 GJCs [18,19], together with the recent structure of Cx31.3 HC [20] provided deep insights into the shared structural features of the connexin channels. These structures hint at the role of the N-terminal domain (NTD) in molecular gating of GJCs and HCs, with several conformations of the NTD observed in different connexin homologues [18-20]. Additionally, biochemical evidence points to the roles in channel gating played by the link between Cx43 intracellular loop and the C-terminal region [21,22]. However, despite the availability of this evidence, the molecular determinants of intracellular connexin channel gating remain unclear. To shed light on the structural basis of Cx43 gating, we set out to determine its structure by cryo-EM and to analyse its dynamics with molecular dynamics (MD) simulations.

Results

Structures of Cx43 GJC and HC in detergent micelles and in nanodiscs. Our Cx43 expression system was tested using electrophysiology in HeLa cells (Figure S1A-D). The experiments confirmed the functionality of Cx43 GJCs expressed in transfected cells. For large-scale protein expression, Cx43 featuring a C-terminal HRV3C-YFP-twinStrep tag, was expressed in adherent mammalian cells (HEK293F) using transient transfection method. The produced protein was purified using affinity and size exclusion chromatography in digitonin (Figure S2A-C) and flash frozen on cryo-EM grids. The grids were subjected to single particle cryo-EM analysis (Figure S3), yielding the final 3D reconstruction at 2.26 Å resolution (Figure 1A, Figure S3-4).

The overall architecture of the protein complex resembles that observed with other connexin GJCs, with two hemichannels (connexons) from adjacent plasma membrane regions coupled to form a full GJC (Figure 1A-B). The exterior of the channel is decorated by several ordered lipid-like density elements (Figure 1A-B), reminiscent of the previously observed lipids bound at the protein-bilayer interface in other connexins [19]. In the case of Cx43, the lipid-like densities appear to decorate the protein-lipid bilayer interface at both the inner and the outer leaflet of the membrane. Comparison of the Cx43 monomers to the available structures of Cx26 and Cx46 GJCs and the Cx31.3 HC revealed a major difference in the NTD arrangement in these channels (Figure 1C-D). The conformation of the NTD in the Cx31.3 HC structure appears to be the closest to that in Cx43 GJC. Analysis of the tryptic peptides revealed that most of the protein lacks the residue M1 (Figure S5), and thus the model was built starting with G2.

To ascertain that the conformation of Cx43 GJC is not induced by the detergent present in the sample we removed the detergent and reconstituted the protein into MSP2N2 nanodiscs, using 1-palmitoyl-2-oleoyl-glycero-3-phosphocholine (POPC) as a mimic for the native lipid environment. The reconstituted protein was subjected to the same imaging and analysis workflow as Cx43 GJC in digitonin. The 2D classes of the MSP2N2-reconstituted Cx43 showed features consistent with a mixture of GJCs and HC. Processing of the corresponding particles resulted in 3D reconstructions of the Cx43 GJC at 2.95 Å resolution (Figure S6, S8) and HC in nanodiscs at 3.98 Å resolution (Figure 1E-F, Figure S7, S8). The GJCs in detergent and in nanodiscs are nearly identical, with an RMSD of 0.97 Å between the aligned Cx43 monomers (Figure 1G, Figure S9A). Although the differences between the HC in nanodisc and the GJC are more pronounced (Figure S9A), the conformation of the cytosolic region and the NTD is highly conserved (Figure 1G).

Sieve-like gate conformation in Cx43. The reconstructed gate region of Cx43 shows several narrow openings connecting the pore vestibule and the pore interior: a single ~6-7 Å wide central gate (CG) and six adjacent peripheral gates (PG) of similar dimensions (Figure 2A-B). This sieve-like arrangement of the gate region is distinct from any of the previously observed states of connexin GJCs or HCs. This particular gate conformation is established through an interplay of two structural elements: the NTD and the TM2 (Figure 2C-D). The NTD of Cx43 is arranged near parallel to the membrane plane, in a centre-oriented conformation (Figure 2C). The HC of Cx31.3 assembles in a similar manner, with a well-ordered NTD resolved by cryo-EM (Figure 2C-D). However, the TM2 region of Cx31.3 forms a tight seal with the NTD (Figure 2E). In contrast, the TM2 of Cx43 is shifted away from the pore centre, creating six PG openings (Figure 2F). This arrangement of the NTD appears to be stabilized by a small molecule: a density element likely corresponding to a bound small molecule is present within the PG region, wedged between the adjacent NTDs (Figure 2G). Thus, although the conformation of the Cx43 gate is sieve-like, the PG is blocked by a yet unidentified small molecule (which we refer to as the PG lipid, or PGL).

In addition to the PGL molecules stabilizing the NTD arrangement, the cryo-EM density of Cx43 GJC features several well resolved densities inside the pore region (lipid-1 and lipid-2, Figure 2H). These elements likely correspond to bound sterol molecules, such as cholesterol co-purified with the protein from the mammalian cells or cholesterol hemisuccinate (CHS) added to the solubilization mixture during protein extraction from the membrane. Similar densities are present in the Cx43 GJC reconstruction in nanodiscs, in the absence of detergent molecules (Figure S10A).

Identification of the lipid-like molecules bound to Cx43 is a significant challenge. Despite the high overall resolution of the 3D reconstruction of the Cx43 GJC (2.24 Å resolution in detergent and 2.95 Å in nanodisc; Figure S3, S6), the cryo-EM map features in regions corresponding to the lipid densities are insufficient to assign the lipid identity unambiguously.

135 To determine the identities of these lipids experimentally, we performed lipidomic analysis of
136 the organic extracts prepared from the purified Cx43 samples and compared them to the mock
137 control (extracts of prepared from eluates of the purification procedure using cells that do not
138 overexpress the protein as starting material). The results showed that several types of
139 phospholipids, as well as cholesterol were present in both samples. The only lipid-like
140 compound specifically enriched in the purified sample was dehydroepiandrosterone (DHEA;
141 Figure S10B). DHEA is a most abundantly expressed neurosteroid known to modulate ligand-
142 gated ion channels, such as $GABA_A$ [23] or NMDA and AMPA receptors [24]. Although we are
143 presently not able to conclusively state that DHEA corresponds to any of the densities present
144 in our reconstruction, its enrichment in the sample is an interesting observation that deserves
145 detailed future investigations.

146 **Cx43 junction interface.** As in other connexins, the Cx43 GJC interface is formed by two
147 extracellular loops, ECL1 and ECL2 (Figure 3A-B). The portion of the ECL1 comprising
148 residues N55-Q58 makes contacts with two Cx43 monomers from the opposite membrane,
149 with N55-Q58 of one monomer and Q58'-P59' of the neighboring monomer within 4 Å
150 distance (Figure 3C, *top left*). The ECL2 region that directly participates in sealing the junction
151 includes residues P193-D197. Comparisons of the junction-forming loops in Cx43 to those in
152 Cx46 (Figure 2C, *middle*) and Cx26 (Figure 2C, *right*) show that each protein uses a similar
153 pattern of inter-HC interaction within each GJC. It is noteworthy that both the amino acid
154 sequences (Figure 3D) and the interaction networks (Figure 3C) are similar in the ECL1 for
155 Cx43 and Cx46, and in the ECL2 for Cx46 and Cx26. The differences in these two loops, and
156 especially in ECL2, underlie the inability of Cx43 (which has been grouped into a docking
157 group 2) to engage in heterotypic interactions with group 1 connexins (such as Cx46 and Cx26)
158 [25]. Our structure is thus in line with the recognized consensus motif necessary for heterotypic
159 complementarity of connexin GJCs [26].

160 **Conformation of the Cx43 hemichannel.** Although the two Cx43 GJC structures (in detergent
161 micelles and in nanodiscs) are almost identical, the Cx43 HC shows a notable difference in the
162 ECL1-2 conformation (Figure 3E-F). The resolution of the HC reconstruction does not allow
163 us to make definitive statements about the orientations of individual side chains, but it is clear
164 that both loops engaging in junction formation move inward upon docking of the two HCs
165 (Figure 3F). This conformational change likely involves intra- and intermolecular
166 cooperativity. The ECL1 and ECL2 are linked via several disulphide bonds, and thus the
167 rearrangement within each molecule would require concerted movement of the whole
168 extracellular domain (ECD). The ECD movement within one monomer is likely cooperatively
169 coupled to the neighboring chains within the Cx43 HC.

170 **Disease-linked mutations in Cx43.** A number of disease-linked mutations associated with
171 Cx43 can be mapped directly to three regions of interest revealed by our structures: (i) the GJC
172 intra-pore lipid-like site, (ii) the ECD, and (iii) the gating region (Figure 4A). The interior of
173 the channel features two lipid-like densities (Figure 2H, 4B; Figure S4E, S10A). The observed
174 position of lipid 1 is consistent with the previously found phospholipid-like densities inside the
175 pore of the Cx31.3 HC [20]. Lipid 2 inserts into the pocket formed by TM1 and TM2, parallel
176 with the NTD. Unlike Cx31.3, where elongated densities within the pore region could be
177 interpreted as hydrophobic tails of bound phospholipids, the density in the Cx43 GJC appears
178 consistent with that of a sterol (Figure 2H, 4B). The presence of a small hydrophobic small
179 molecule in Cx43 at this site suggests a potential mechanism of lipid-based Cx43 regulation,
180 whereby binding of a lipid could directly influence the conformation of the gating elements of
181 the protein (such as NTD). An effect of a cholesterol analogue 7-ketocholesterol on Cx43
182 permeability has been observed previously [27], and such an effect may be mediated via the
183 binding sites within the GJC (or HC) pore (Figure 4B; Figure S10A). The presence nearby of

184 several residues known to be linked to ODDD when mutated (S27P, I31M[28], S86Y[29], L90V[10])
185 points to a potential functional significance of the intra-pore lipid binding site.

186 Two known mutations linked to ODDD are located in the Cx43 ECD: P59 in ECL1 [30] and
187 H194 in ECL2 [31]. As suggested by the Cx43 GJC structures, these residues are located in
188 conserved regions where any substitution can be expected to cause disruption of the contacts
189 critical for junction formation (Figure 4C).

190 Multiple mutations in Cx43 associated with ODDD are located in the N-terminus (G2V, D3N,
191 L7V, L11I/P, Y17S, S18P), the TM1 region (G21R, G22E, K23T) and the TM2 region
192 proximal to the gate (V96M/E/A, Y98C, K102N) [11]. In some cases, the mutations reduce the
193 ability of Cx43 to form the gap junction plaques at the plasma membrane, as is the case for
194 Y17S or G21R (as well as L90V, located at the pore lipid binding site) [32]. The mutations tend
195 to have deleterious effects on the permeability of Cx43 to ions and small molecules [11].
196 Interestingly, a G8V amino acid substitution has been linked to palmoplantar keratoderma and
197 congenital alopecia 1 (PPKCA1). This mutant can form functional gap junctions and has
198 enhanced HC activity [33]. Mapping these sites on the structure of Cx43 allows us to gain insights
199 into the possible mechanisms that underlie the associated disorders (Figure 4D-E). For
200 example, channel blockage or hyperpermeability due to mutations in or around the gating
201 region may link Cx43 to diseases.

202 To test the functional consequences of mutations in the gating region, and in particular in the
203 PG region, we introduced several single residue substitutions in the NTD (A6F, G8F, G8V)
204 and TM2 (R101W) of Cx43. The mutations were designed to introduce bulky hydrophobic
205 side-chains into the locations that may perturb the integrity of the PG: either obstructing the
206 PG or preventing the PGL from binding to it, which could in turn influence the GJC transport.
207 We tested the ability of the mutated proteins to form functionally active GJCs in fluorescence
208 recovery after photobleaching (FRAP) assays in HEK293F cells expressing the mutant
209 proteins. Cx43 and the mutants could be expressed and showed expression patterns consistent
210 with gap junction formation between the neighbouring cells (Figure S11). Each of the tested
211 mutant variants of Cx43 retained the ability to transport a small molecule substrate,
212 sulforhodamin-101 (Figure S12). As noted above, the PPKCA1-linked mutant G8V has been
213 shown to form hyperactive HCs, and thus the lack of its effect on GJC function is not
214 unexpected. None of the other mutations were sufficient to disrupt the basic function of Cx43
215 GJCs in transporting the large substrates. Thus, although we can visualize the locations of the
216 disease-linked mutations, the underlying causes of the disease phenotypes will require more
217 detailed future investigations. Within the scope of this study, one can conclude that
218 introduction of bulky residues in the positions 6, 8 and 101 does not affect the transport function
219 of Cx43.

220 **Molecular dynamics simulations of Cx43 GJC.** Based on our model of Cx43, the dimensions
221 of the CG are likely incompatible with the translocation of a larger molecule, such as ATP,
222 cAMP or IP3 (typical substrates of Cx43 GJC-mediated transport). To assess the permeability
223 of the gate to ions, we performed MD simulations. We performed four independent molecular
224 dynamics simulations of the Cx43 GJC embedded in a double POPC bilayer solvated in 150
225 mM KCl (Figure 5A). Given the ambiguity in the lipid identity and binding mode, no potential
226 lipid surrogates were included inside the pore or NTD region. After equilibration (detailed in
227 Materials and Methods) the dodecameric structure was stable in all simulations, as indicated
228 by the small root mean square deviation (RMSD, Figure 5B; Figure S13).

229 As noted above, the CG pore has a solvent accessible radius very close to the effective hydrated
230 radius of K^+ (~6.6 Å) and Cl^- (~7.2 Å). The NTD regions of Cx43 are flexible and can move
231 laterally and vertically (Movie S1), allowing the passage of ions. The charge distribution inside
232 Cx43 resembles that of the other GJCs [18,19,34] with a positive electrostatic potential in the NTD

region of both HCs within a channel and a negative/neutral region near the HC interface (Figure 5C). When no transmembrane potential is applied (0 mV, Figure 5D), Cl^- ions accumulate in the NTD regions of Cx43 GJC (negative free-energy in the NTD region) as previously observed for C31.3 [34]. At 0 mV, there is a of ~2 kcal/mol barrier for cations (K^+) while no barrier is found for anions. Cations get trapped between the two NTD barriers, and no full translocations are observed during the simulation time at 0 mV because the gates remain closed. Upon application of transmembrane voltage, the barrier on one HC lowers and full translocations are observed (Figure 5D; detailed balance is provided in Table S2).

Interestingly, the GJC did not fully open in any of our simulations, i.e., a conformation with all NTDs within the channel symmetrically moving to open the pore was not established at any point. However, voltage-induced fluctuations of the individual NTDs allow the ions to pass. To illustrate this effect we calculated the angle formed by the NTD and TM1 for all of the chains in each of simulation (Figure 6A-D). We assessed the difference between the open conformation (θ ~25º), the initial cryo-EM structure in the closed conformation (θ ~75º) and the angle after equilibration (θ ~55º) in all of our simulations (Figure 6B). At 0 mV the NTD fluctuates in different intermediate positions but is never fully open (Figure 6C). Only at high applied transmembrane voltages the NTD fully folds inwards, thus opening the channel (Figure 6D). This is an important observation, taking into account the six-fold symmetry of the connexin channels: although our understanding of the channel structure implies a symmetrical arrangement of all its subunits, the gating events under physiological conditions, and under the MD conditions as shown here, may involve asymmetrical conformational changes within the NTD or other regions of the GJC or HC.

The MD simulations confirm that the structure is closed and semi-permeable to ions, even in the absence of the PGL molecules occupying the gating region. Ion conductance only occurs upon voltage application and is gated by the NTD regions folding inwards toward an open-like conformation. The open NTD conformations of individual Cx43 monomers forming under high voltage conditions in our MD simulations are similar to the open NTD conformations previously reported using experimental approaches [17,18].

Discussion

The structures of Cx43 we have obtained by cryo-EM reveal a novel conformation of a connexin channel (both GJC and HC) featuring a closed sieve-like molecular gate. The state is distinct from the previously observed structures of connexin GJCs and HCs, adding an important missing component to our understanding of connexin-mediated intercellular communication. With these structures in mind, we can now establish the existence of several structurally defined gating substates of the connexin channels: (i) a fully open gate, (ii) a semi-permeable central gate, and (iii) a closed sieve-like gate (Figure 7). The gating mechanisms of connexin HCs and GJC are complex and involve multiple components. The available evidence indicates that connexin channels are gated by membrane potential (V_m), by transjunctional potential (V_t), as well as by a range of chemical agents such as pH, Ca^{2+} and organic molecules [35]. For example, a ball-and-chain model has been proposed for Cx26, whereby at low pH the NTDs extend deep into the pore and occlude the substrate translocation pathway [36]. This conformation is distinct from the one captured by our cryo-EM reconstructions, and it is possible that under certain conditions the Cx43 NTD may transition from a sieve-like conformation to a low pH Cx26-like state.

The cytosolic surface of the gate in our structures is positively charge, indicating that specific interaction with anions may be relevant to some of the gating events. As Cx43 is capable of cation and anion permeation [37], the presence of the positively charged surface in this region does not indicate ion selectivity. The differences in the electrostatic properties of the gates and

282 the pore regions in different connexin channels may reflect the differences in their selectivity
283 for ions and small molecules (Figure S14). However, it is also likely that the unstructured
284 regions in Cx43 and other connexins, including the intracellular loop and the C-terminal
285 domain, contribute to the electrostatic potential, substrate selectivity and regulation of these
286 channels. These domains are known to play important roles in connexin channel regulation [38].
287 However, as these regions are unresolved in any of the available 3D reconstructions of
288 connexin channels, the structural basis of their action remains to be determined.

289 The observation of lipid-like molecules bound inside the pore is intriguing. The use of
290 detergents and lipids is currently a prerequisite for structural analysis of membrane proteins,
291 and it is possible that under solubilization conditions the abundance of added detergent and
292 lipid (CHS) forces the protein to interact with these molecules. Nevertheless, these interactions
293 may correspond to the naturally occurring interactions with the endogenous lipids present in
294 the lipid bilayer of the cell. The presence of such molecules could have important implications
295 for HC or GJC assembly, substrate permeation and molecular gating. It remains to be
296 determined whether Cx43 or other connexin channels harbour intra-pore lipids in the cellular
297 membranes *in vivo*.

298 Distinct gating modes have been shown in the literature for both Cx43 HCs and GJCs, with
299 fast transitions from an open state to a state of residual conductance, and slow transitions from
300 an open to a fully closed state [35]. The structures of Cx43 described here likely represent the
301 fully closed states, observed previously by electrophysiological recordings. This state could be
302 stabilized by a yet unknown agent that occludes the PG opening formed by the arrangement of
303 the NTDs and TM2 regions observed in our structures. Detailed investigations of Cx43 and
304 other connexin channels will be required to determine whether the sieve-like gate conformation
305 is a common feature among different GJCs and HCs, and to pinpoint the physiological
306 circumstances that establish this gating conformation.

307

Acknowledgements

We thank Emiliya Poghossian (EM Facility, PSI) and Miroslav Peterek (ScopeM, ETH Zurich) for expert support in cryo-EM data collection. We also thank Spencer Bliven and Marc Caubet-Serrabou (PSI) for the support in high performance computing. The work was supported by a grant from Horten Foundation, and by the Swiss National Science Foundation grant 184951 (VMK). FLG and SAG thank the CSCS and PRACE for supercomputing resources (projects pr126 and s1107).

Competing interests

Authors declare that they have no competing interests.

Data and materials availability

The atomic coordinates and structure factors have been deposited in the Protein Data Bank (7Z1T, 7Z22, 7Z23); the density maps have been deposited in the Electron Microscopy Data Bank (EMD-14452, EMD-14455, EMD-14456). The mass spectrometry data will be deposited at ProteomeXChange via PRIDE. All other data are available in the main text or the supplementary materials.

Author contributions

C.Q. planned and performed the experiments, analyzed the data, wrote the manuscript, S.A.G. planned, performed and analyzed the simulations, co-wrote the manuscript, P.L. performed the experiments, co-wrote the manuscript, A.O. performed the experiments, analyzed the data, D.L.P. performed the experiments, analyzed the data, E.B. performed the experiments, analyzed the data, D.S. performed the experiments, analysed the data, co-wrote the manuscript, P.P. provided the reagents, equipment and expertise for mass spectrometry experiments, N.Z. provided the reagents, equipment and expertise for lipidomics analysis, M.B. planned the experiments, analyzed the data, co-wrote the manuscript, F.L.G. planned and analyzed the simulations, co-wrote the manuscript, V.M.K. planned and performed the experiments, analyzed the data, wrote the manuscript.

Figures

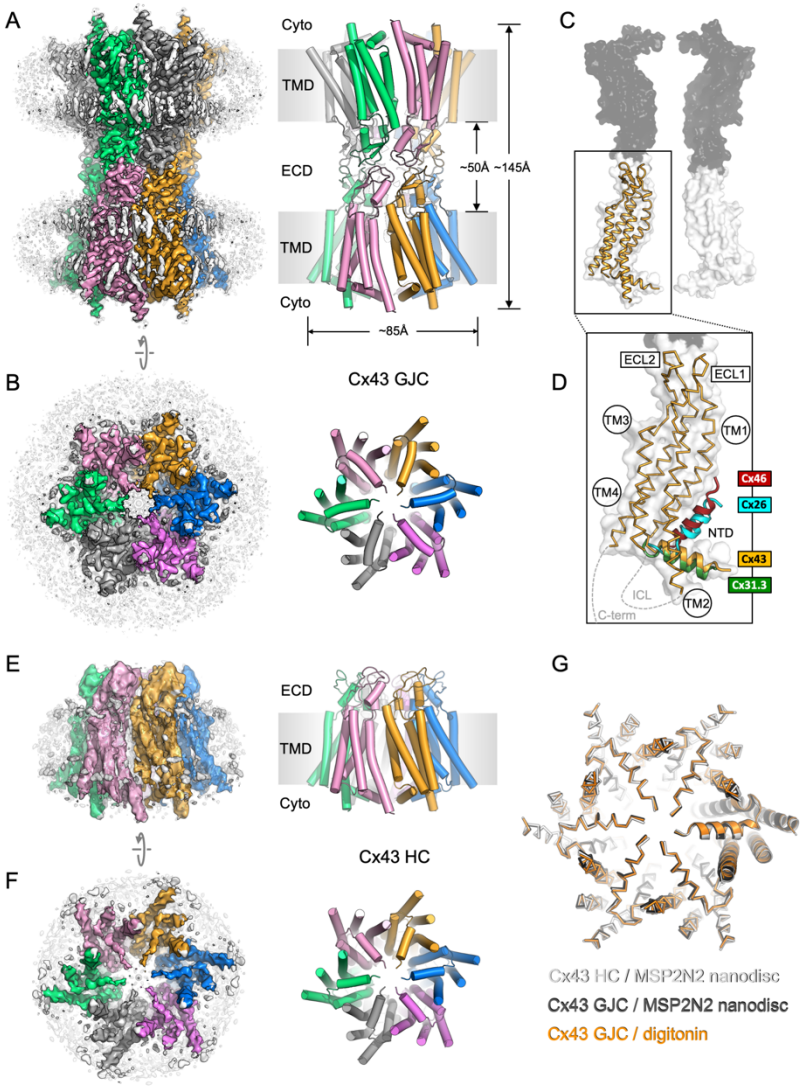

Figure 1. Structure of human Cx43 gap junction channel. A-B, Cryo-EM density map and model of Cx43 GJC solved by cryo-EM at 2.26 Å resolution. The individual Cx43 monomers in each HC within the GJC are coloured blue, pink, grey, green, salmon and orange. Grey densities correspond to the detergent micelle and the bound sterol-like molecules. **C**, The position of a single Cx43 monomer (orange) within a GJC (represented as a surface of juxtaposed Cx43 monomers in two distinct membrane regions, white and grey). **D**, Alignment of the monomers of Cx43, Cx26 (PDB ID: 2zw3), Cx46 (PDB ID: 7jkc) and Cx31.3 (PDB ID: 6l3t) shows the distinct orientations of the N-terminal domain ("NTD") helix. Individual TM domains, extracellular loops 1 and 2 ("ECL1-2"), relative positions of the intracellular loop ("ICL") and the C-terminus ("C-term") are indicated. **E-F**, Same as A-B, for the Cx43 HC in MSP2N2 nanodiscs at 3.98 Å resolution. **G**, Alignment of three indicated structures shows that the conformation of the gating region is highly conserved. The models are shown as ribbons; one of the aligned monomers in each of the structures is represented as cartoon, to clearly indicate the monomer boundaries.

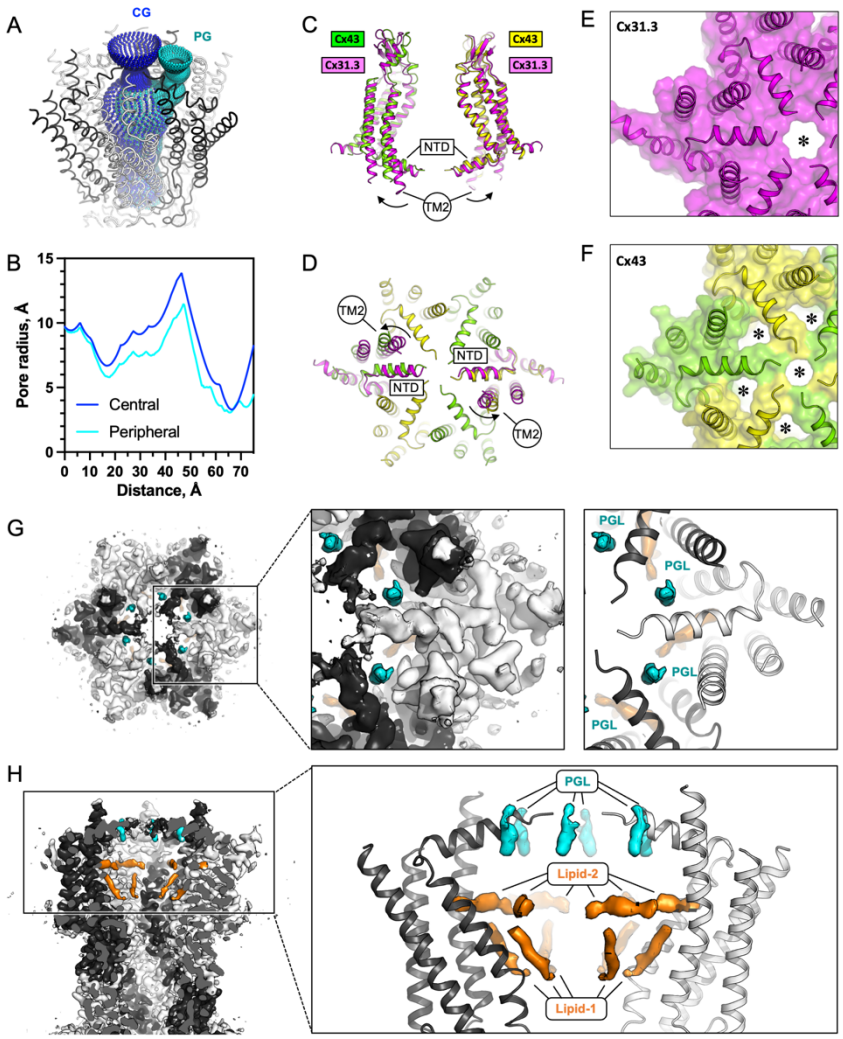

Figure 2. The Cx43 gate adopts a sieve-like conformation. A-B, Pore analysis using HOLE reveals a constriction of the pore at the gate. Only a central opening and one of the peripheral openings within one HC of Cx43 GJC in digitonin is shown. The distance is calculated from the center of the GJC pore to a point outside of the channel. Central gate ("CG") and peripheral gate ("PG") regions are indicated in the panel. **C-D**, Comparison of the Cx43 in digitonin with the Cx31.3 HC shows that the peripheral gate opening is created by the particular arrangement of the NTD and by adjustment of the TM2. **E-F**, The distinct NTD/TM2 arrangement results in a single pore opening in the structure of Cx31.3 (indicated with an asterisk, E), contrary to Cx43 (F). **G**, A view of the Cx43 gating region from the cytosol reveals the location of the PG lipids ("PGL") stabilizing the NTD arrangement, shown as isolated PGL densities (cyan). **H**, A slab view of the gating region parallel to the membrane plane shows the relative arrangement of the PGLs and the intra-pore lipids ("Lipid-1" and Lipid-2"; orange).

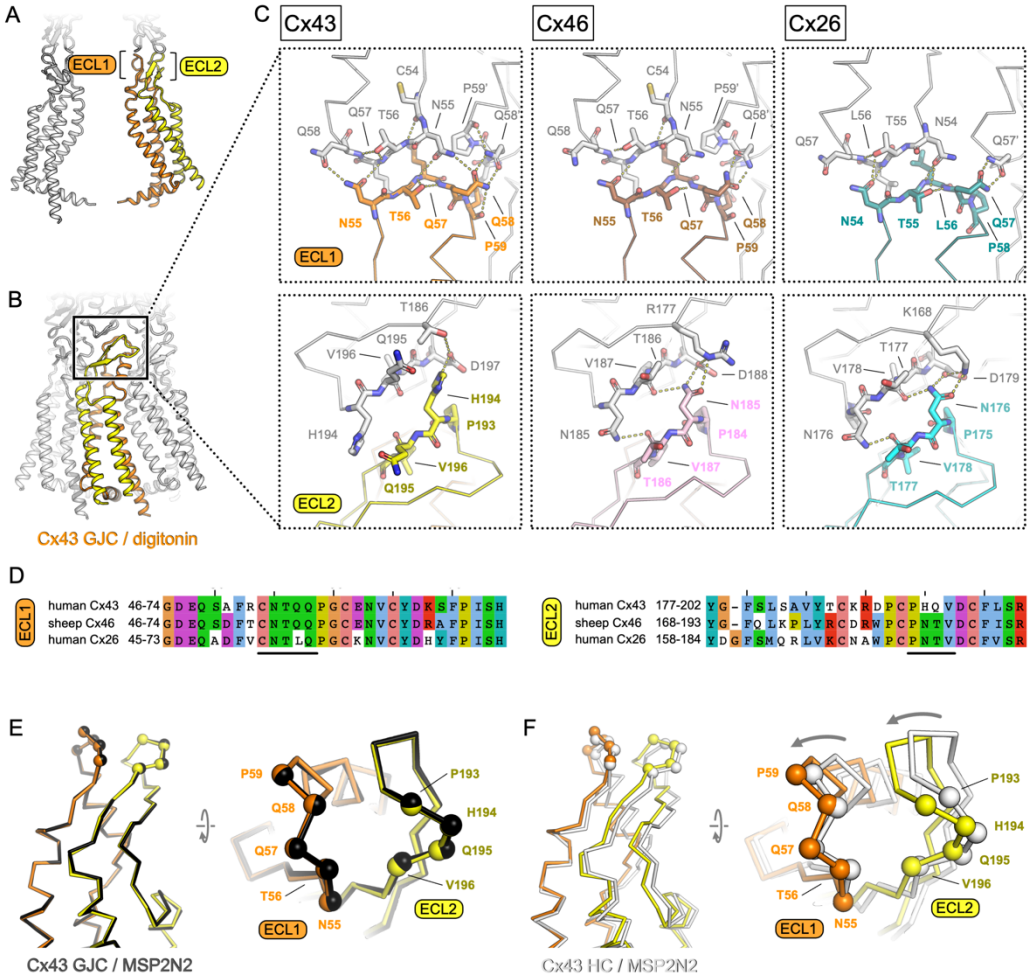

Figure 3. Extracellular domain of Cx43 GJC and HC. A-B, The lateral views of Cx43 GJC in digitonin, indicating the positions of the extracellular loops 1 and 2. **C**, Views of the extracellular loops ECL1 (top) and ECL2 (bottom), for Cx43 (left), Cx46, (middle; PDB ID: 7jkc), and Cx26 (right; PDB ID: 2zw3). The residues of one monomer in each of the structures, directly involved in junction formation, are coloured by element with carbon atoms as orange/yellow (Cx43), brown/pink (Cx46) and teal/cyan (Cx26). The residues of the neighbouring connexin monomers within 4 Å distance are shown coloured with white carbon atoms. Dotted lines indicate electrostatic contacts, calculated in PyMol. **D**, Sequence alignment of the complete ECL1 and ECL2 regions of the three proteins shown in C. The black lines indicate the GJC interface residues, as shown in C. **E**, Alignment of the Cx43 GJC structures in digitonin micelles and in nanodiscs. Cα atoms of the interface residues shown in C are represented as spheres (the ribbon and spheres of Cx43 in nanodiscs is coloured black). **F**, Same as E, for a comparison between Cx43 GJC in digitonin and Cx43 HC in nanodiscs. The arrow indicates the movement of the two loops that accompanies GJC formation. The ribbon and spheres of Cx43 HC are light grey.

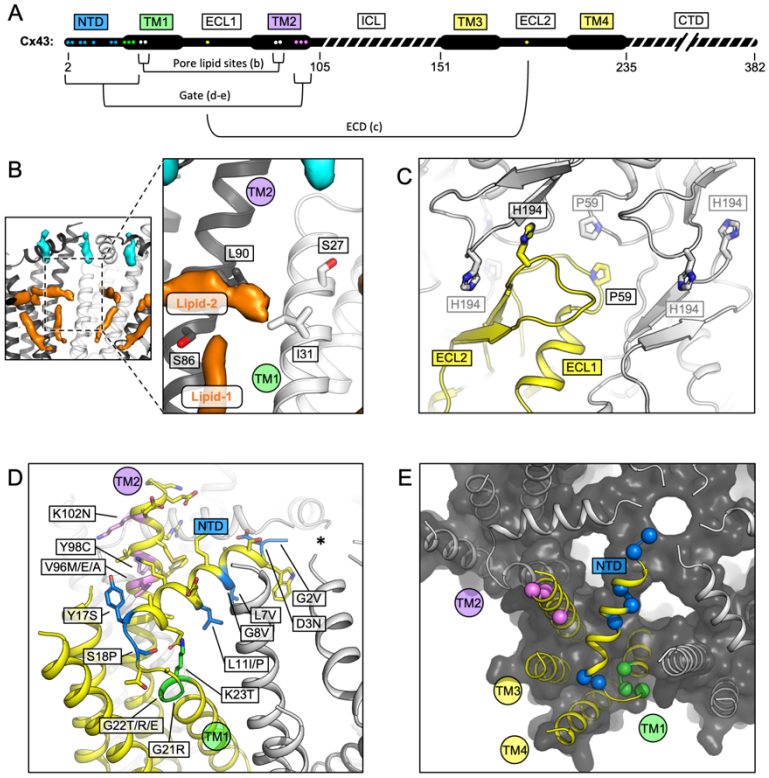

Figure 4. Locations of the disease-linked mutations in the Cx43 GJC structure. A, Disease-linked mutations mapped on the sequence of Cx43. The amino acid residues proximal to the intrapore lipid densities ("Pore lipid sites") are shown as white dots. The residues at the GJC interface are shown as yellow dots ("ECD"). The residues of the gating region ("Gate") are shown as blue (NTD), green (TM1) and violet (TM2) dots. The sequence elements not resolved in our 3D reconstruction are indicated with a dashed line. **B**, Two sterol-like density elements (Lipid-1 and -2) are located within the pore region of Cx43 GJC (white). The indicated disease-linked mutations are located within close distance of the pore lipid densities. **C**, A view of the extracellular loops forming the junction, indicating two residues known to be linked with ODDD, P59 and H194 (side chains shown as sticks; one of the monomers in the GJC is coloured yellow). **D**, A view of the gating region with the highlighted disease-linked mutations, colored as in A. **E**, A similar representation of the disease-linked mutations, with Cα atoms shown as spheres, illustrating the contribution of the mutants to gate formation.

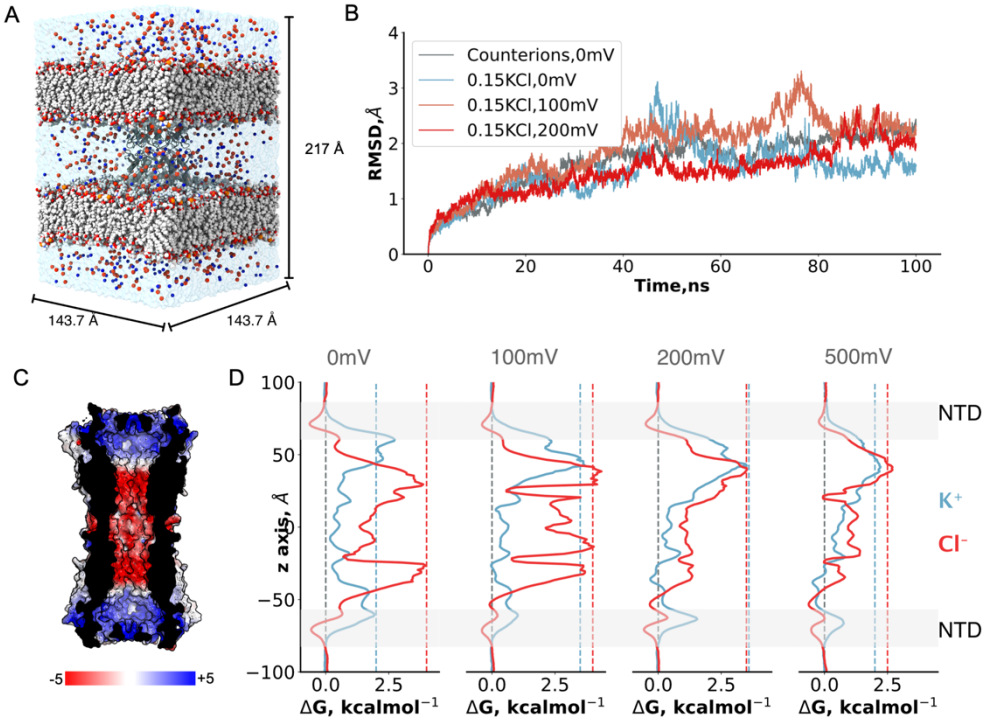

Figure 5. Molecular dynamics simulations of the Cx43 GJC. A, Molecular dynamics simulation box. **B**, C_α root-mean-square-deviation from the cryo-EM structure during the different molecular dynamics simulations. **C**, The surface representation of Cx43 coloured according to the calculated electrostatic potential; the slab view shows the properties of the pore. **D**, Free energy experienced by the K^+ (blue) and Cl^- (red) while permeating the pore with different applied transmembrane potential. The dotted lines correspond to the maximum free energy barrier for anions (red) and cations (blue); black dotted line corresponds to the baseline.

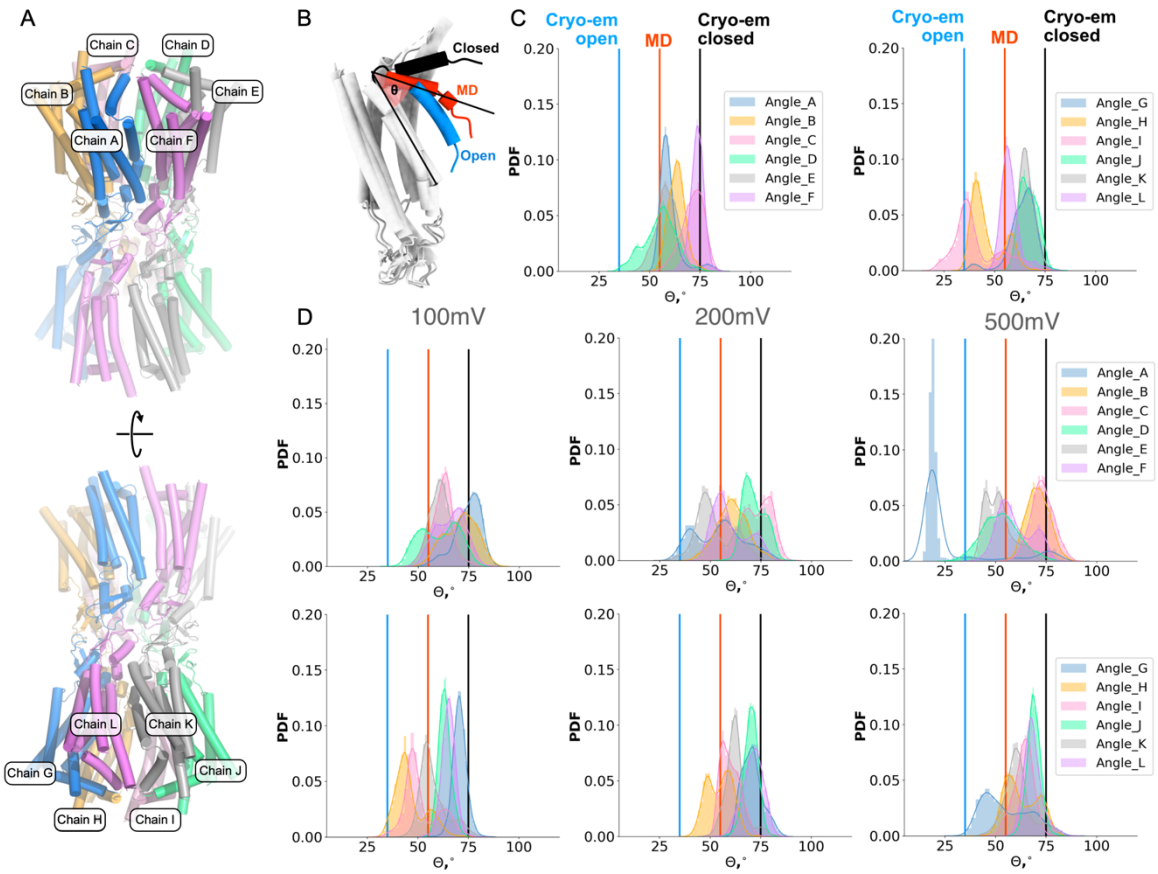

Figure 6. Molecular dynamics simulations reveal voltage-dependent partial opening of the gate. A, Views of a GJC, with twelve chain names referred to in c-d indicated. **B**, Superimposition of a single chain depicted as cartoon for the closed structure of Cx43 (NTD coloured in black), a semipermeable (rare) state extracted from the molecular dynamics simulation (NTD coloured red) and the open structure of Cx46 (PDB ID: 7jjp, NTD coloured blue). The angle θ corresponds to the calculated angle of the NTD domain with respect to TM1. **C**, Population density of the NTD opening angle, θ, for the different chains in the GJC during MD at 0 mV. **D**, The same analysis as in c, for the independent simulations with different applied transmembrane voltages, for chains A to F (*top*) and for chains G to L (*bottom*).

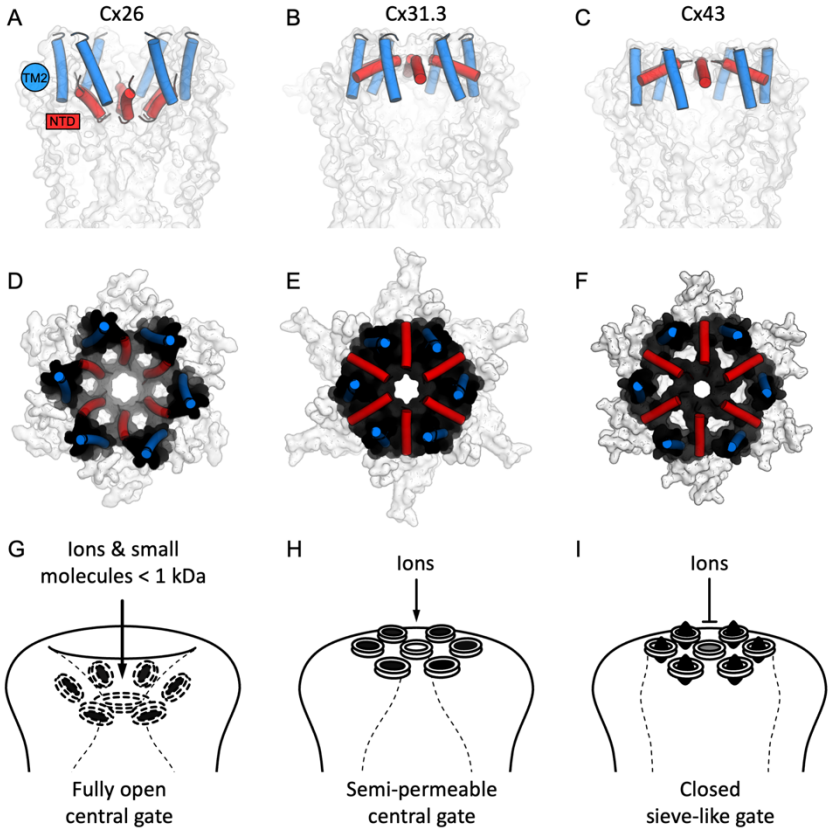

Figure 7. A structure-based view of connexin gating states. A, The side view of a fully open gate, as observed in Cx26 GJC (PDB ID: 2zw3); the gate-forming regions of the protein, NTD (red) and TM2 (blue), are shown as cylinders. Similar arrangement of the gating elements has been observed in Cx46/Cx50. This conformation of the gate is permeable to a wide range of substrates, including small molecules and ions. **B**, The semi-permeable central gate is featured in the structure of Cx31.3 HC (PDB ID: 6l3t). In this conformation the gate is likely selective for ions (Cx31.3 has been shown to have a preference for anions), based on the dimensions of the gate. **C**, The sieve-like closed gate is featured in the Cx43 structures (here, the Cx43 in digitonin is shown as an example). **D-F**, Same as A-C, viewed from the cytosolic side of the channel. The black surface corresponds to the NTD and TM2 regions; the white surface corresponds to the rest of the protein. **G-I**, A schematic representation of the three gating states of connexin channels.

445 **References**
446

447 1 Churko, J. M. & Laird, D. W. Gap junction remodeling in skin repair following
448 wounding and disease. *Physiology (Bethesda)* **28**, 190-198,
449 doi:10.1152/physiol.00058.2012 (2013).
450 2 Liang, Z. *et al.* The Multifaceted Role of Astrocyte Connexin 43 in Ischemic Stroke
451 Through Forming Hemichannels and Gap Junctions. *Front Neurol* **11**, 703,
452 doi:10.3389/fneur.2020.00703 (2020).
453 3 Poelzing, S. & Rosenbaum, D. S. Altered connexin43 expression produces arrhythmia
454 substrate in heart failure. *Am J Physiol Heart Circ Physiol* **287**, H1762-1770,
455 doi:10.1152/ajpheart.00346.2004 (2004).
456 4 Rodriguez-Sinovas, A., Sanchez, J. A., Valls-Lacalle, L., Consegal, M. & Ferreira-
457 Gonzalez, I. Connexins in the Heart: Regulation, Function and Involvement in Cardiac
458 Disease. *Int J Mol Sci* **22**, doi:10.3390/ijms22094413 (2021).
459 5 Syrjanen, J., Michalski, K., Kawate, T. & Furukawa, H. On the molecular nature of
460 large-pore channels. *J Mol Biol*, 166994, doi:10.1016/j.jmb.2021.166994 (2021).
461 6 Srinivas, M., Verselis, V. K. & White, T. W. Human diseases associated with connexin
462 mutations. *Biochim Biophys Acta Biomembr* **1860**, 192-201,
463 doi:10.1016/j.bbamem.2017.04.024 (2018).
464 7 Beyer, E. C., Paul, D. L. & Goodenough, D. A. Connexin43: a protein from rat heart
465 homologous to a gap junction protein from liver. *J Cell Biol* **105**, 2621-2629,
466 doi:10.1083/jcb.105.6.2621 (1987).
467 8 Robertson, J. D. The Occurrence of a Subunit Pattern in the Unit Membranes of Club
468 Endings in Mauthner Cell Synapses in Goldfish Brains. *J Cell Biol* **19**, 201-221,
469 doi:10.1083/jcb.19.1.201 (1963).
470 9 Laird, D. W. & Lampe, P. D. Therapeutic strategies targeting connexins. *Nat Rev Drug*
471 *Discov* **17**, 905-921, doi:10.1038/nrd.2018.138 (2018).
472 10 Paznekas, W. A. *et al.* Connexin 43 (GJA1) mutations cause the pleiotropic phenotype
473 of oculodentodigital dysplasia. *Am J Hum Genet* **72**, 408-418, doi:10.1086/346090
474 (2003).
475 11 Paznekas, W. A. *et al.* GJA1 mutations, variants, and connexin 43 dysfunction as it
476 relates to the oculodentodigital dysplasia phenotype. *Hum Mutat* **30**, 724-733,
477 doi:10.1002/humu.20958 (2009).
478 12 Wiest, T. *et al.* Clinical and genetic variability of oculodentodigital dysplasia. *Clin*
479 *Genet* **70**, 71-72, doi:10.1111/j.1399-0004.2006.00631.x (2006).
480 13 Dasgupta, C. *et al.* Identification of connexin43 (alpha1) gap junction gene mutations
481 in patients with hypoplastic left heart syndrome by denaturing gradient gel
482 electrophoresis (DGGE). *Mutat Res* **479**, 173-186, doi:10.1016/s0027-
483 5107(01)00160-9 (2001).
484 14 Pizzuti, A. *et al.* A homozygous GJA1 gene mutation causes a Hallermann-
485 Streiff/ODDD spectrum phenotype. *Hum Mutat* **23**, 286, doi:10.1002/humu.9220
486 (2004).
487 15 Ribeiro-Rodrigues, T. M., Martins-Marques, T., Morel, S., Kwak, B. R. & Girao, H. Role
488 of connexin 43 in different forms of intercellular communication - gap junctions,
489 extracellular vesicles and tunnelling nanotubes. *J Cell Sci* **130**, 3619-3630,
490 doi:10.1242/jcs.200667 (2017).

491 16 Unger, V. M., Kumar, N. M., Gilula, N. B. & Yeager, M. Three-dimensional structure of
492 a recombinant gap junction membrane channel. *Science* **283**, 1176-1180,
493 doi:10.1126/science.283.5405.1176 (1999).
494 17 Maeda, S. *et al.* Structure of the connexin 26 gap junction channel at 3.5 A
495 resolution. *Nature* **458**, 597-602, doi:10.1038/nature07869 (2009).
496 18 Myers, J. B. *et al.* Structure of native lens connexin 46/50 intercellular channels by
497 cryo-EM. *Nature* **564**, 372-377, doi:10.1038/s41586-018-0786-7 (2018).
498 19 Flores, J. A. *et al.* Connexin-46/50 in a dynamic lipid environment resolved by
499 CryoEM at 1.9 A. *Nat Commun* **11**, 4331, doi:10.1038/s41467-020-18120-5 (2020).
500 20 Lee, H. J. *et al.* Cryo-EM structure of human Cx31.3/GJC3 connexin hemichannel. *Sci*
501 *Adv* **6**, eaba4996, doi:10.1126/sciadv.aba4996 (2020).
502 21 Xu, Q. *et al.* Gating of connexin 43 gap junctions by a cytoplasmic loop calmodulin
503 binding domain. *Am J Physiol Cell Physiol* **302**, C1548-1556,
504 doi:10.1152/ajpcell.00319.2011 (2012).
505 22 Ponsaerts, R. *et al.* Intramolecular loop/tail interactions are essential for connexin
506 43-hemichannel activity. *FASEB J* **24**, 4378-4395, doi:10.1096/fj.09-153007 (2010).
507 23 Gartside, S. E., Griffith, N. C., Kaura, V. & Ingram, C. D. The neurosteroid
508 dehydroepiandrosterone (DHEA) and its metabolites alter 5-HT neuronal activity via
509 modulation of GABAA receptors. *J Psychopharmacol* **24**, 1717-1724,
510 doi:10.1177/0269881109105836 (2010).
511 24 Kimonides, V. G., Khatibi, N. H., Svendsen, C. N., Sofroniew, M. V. & Herbert, J.
512 Dehydroepiandrosterone (DHEA) and DHEA-sulfate (DHEAS) protect hippocampal
513 neurons against excitatory amino acid-induced neurotoxicity. *Proc Natl Acad Sci U S*
514 *A* **95**, 1852-1857, doi:10.1073/pnas.95.4.1852 (1998).
515 25 Bai, D., Yue, B. & Aoyama, H. Crucial motifs and residues in the extracellular loops
516 influence the formation and specificity of connexin docking. *Biochim Biophys Acta*
517 *Biomembr* **1860**, 9-21, doi:10.1016/j.bbamem.2017.07.003 (2018).
518 26 Koval, M., Molina, S. A. & Burt, J. M. Mix and match: investigating heteromeric and
519 heterotypic gap junction channels in model systems and native tissues. *FEBS Lett*
520 **588**, 1193-1204, doi:10.1016/j.febslet.2014.02.025 (2014).
521 27 Girao, H., Catarino, S. & Pereira, P. 7-Ketocholesterol modulates intercellular
522 communication through gap-junction in bovine lens epithelial cells. *Cell Commun*
523 *Signal* **2**, 2, doi:10.1186/1478-811X-2-2 (2004).
524 28 Richardson, R., Donnai, D., Meire, F. & Dixon, M. J. Expression of Gja1 correlates with
525 the phenotype observed in oculodentodigital syndrome/type III syndactyly. *J Med*
526 *Genet* **41**, 60-67, doi:10.1136/jmg.2003.012005 (2004).
527 29 Jamsheer, A. *et al.* Three novel GJA1 missense substitutions resulting in oculo-dento-
528 digital dysplasia (ODDD) - further extension of the mutational spectrum. *Gene* **539**,
529 157-161, doi:10.1016/j.gene.2014.01.066 (2014).
530 30 Vasconcellos, J. P. *et al.* A novel mutation in the GJA1 gene in a family with
531 oculodentodigital dysplasia. *Arch Ophthalmol* **123**, 1422-1426,
532 doi:10.1001/archopht.123.10.1422 (2005).
533 31 Vitiello, C. *et al.* A novel GJA1 mutation causes oculodentodigital dysplasia without
534 syndactyly. *Am J Med Genet A* **133A**, 58-60, doi:10.1002/ajmg.a.30554 (2005).
535 32 Lai, A. *et al.* Oculodentodigital dysplasia connexin43 mutations result in non-
536 functional connexin hemichannels and gap junctions in C6 glioma cells. *J Cell Sci* **119**,
537 532-541, doi:10.1242/jcs.02770 (2006).

538 33 Wang, H. *et al.* Exome sequencing reveals mutation in GJA1 as a cause of
539 keratoderma-hypotrichosis-leukonychia totalis syndrome. *Hum Mol Genet* **24**, 243-
540 250, doi:10.1093/hmg/ddu442 (2015).
541 34 Hyuk-Joon Lee, H. J., Jaekyung Hyun, Bumhan Ryu, Kunwoong Park, Hyun-Ho Lim,
542 Jejoong Yoo, Jae-Sung Woo. Cryo-EM structure of human Cx31.3/GJC3 connexin
543 hemichannel. *Science Advances* **6** (2020).
544 35 Bukauskas, F. F. & Verselis, V. K. Gap junction channel gating. *Biochim Biophys Acta*
545 **1662**, 42-60, doi:10.1016/j.bbamem.2004.01.008 (2004).
546 36 Khan, A. K. *et al.* A Steric "Ball-and-Chain" Mechanism for pH-Mediated Regulation of
547 Gap Junction Channels. *Cell Rep* **31**, 107482, doi:10.1016/j.celrep.2020.03.046
548 (2020).
549 37 Wang, H. Z. & Veenstra, R. D. Monovalent ion selectivity sequences of the rat
550 connexin43 gap junction channel. *J Gen Physiol* **109**, 491-507,
551 doi:10.1085/jgp.109.4.491 (1997).
552 38 D'Hondt, C., Iyyathurai, J., Himpens, B., Leybaert, L. & Bultynck, G. Cx43-hemichannel
553 function and regulation in physiology and pathophysiology: insights from the bovine
554 corneal endothelial cell system and beyond. *Front Physiol* **5**, 348,
555 doi:10.3389/fphys.2014.00348 (2014).
556